JTTEE5 15:634-639
DOI: 10.1361/105996306X147009
1059-9630/$19.00 © ASM International

Peer Reviewed

Microstructure and Properties of Thermally Sprayed Al-Sn-Based Alloys for Plain Bearing Applications

T. Marrocco, L.C. Driver, S.J. Harris, and D.G. McCartney

(Submitted February 28, 2006; in revised form May 10, 2006)

Al-Sn plain bearings for automotive applications traditionally comprise a multilayer structure. Conventionally, bearing manufacturing involves casting the Al-Sn alloy and roll-bonding to a steel backing strip. Recently, high-velocity oxyfuel (HVOF) thermal spraying has been used as a novel alternative manufacturing route. The present project extends previous work on ternary Al-Sn-Cu alloys to quaternary systems, which contain specific additions for potentially enhanced properties. Two alloys were studied in detail, namely, Al-20wt.%Sn-1wt.%Cu-2wt.%Ni and Al-20wt.%Sn-1wt.%Cu-7wt.%Si. This article will describe the microstructural evolution of these alloys following HVOF spraying onto steel substrates and subsequent heat treatment. The microstructures of powders and coatings were investigated by scanning electron microscopy, and the phases were identified by x-ray diffraction. Coating microhardnesses were determined under both as-sprayed and heat-treated conditions, and by the differences related to the microstructures that developed. Finally, the wear behavior of the sprayed and heat-treated coatings in hot engine oil was measured using an industry standard test and was compared with that of previous work on a ternary alloy.

Keywords Al-Sn-based alloys, high-velocity oxyfuel spraying, microstructural characterization

1. Introduction

Plain journal bearings for high-output automotive engine applications are commonly designed against frictional overheating. Although attempts are made to minimize the friction associated with the sliding movement of the bearings by maintaining a continuous film of lubricant between the sliding surfaces, direct contact between the crankshaft and the bearing surface is unavoidable under actual conditions of bearing operation. Frictional heating and temperature increase, resulting from metal-to-metal contact, may lead to the wear of the bearing surface and even of the shaft (Ref 1). Consequently, bearing materials must possess a complex balance of properties.

The composite microstructure for a conventional AlSn-based bearing system (containing typically 12–20 wt.% Sn) comprises a moderate-strength matrix of Al with a dispersion of isolated soft-phase regions of pure Sn, which improve the inherently poor compatibility, conformability, and embedability of the Al. As well as possessing good antifriction characteristics, bearings also need to be capable of withstanding cyclic loading (i.e., fatigue), corrosion, and temperatures in excess of 150 °C in modern engines. However, binary Al-Sn alloys have a limited fatigue strength, and this requires the introduction of additional elements, typically 1 wt.% Cu, to strengthen the αAl matrix through a solid solution hardening and Si, which has beneficial effects on compatibility and wear resistance by forming second-phase hard particles (Ref 2, 3).

The conventional bearing system consists of a multilayer material structure with the Al-Sn-based alloy bonded to a steel backing; the most common manufacturing route for this is the casting and roll-bonding process, with others being powder rolling and continuous casting of the Al alloy onto a steel strip (Ref 2). Postrolling annealing treatments are used to develop a complete diffusion bonding from the initial weld sites and to recrystallize the bearing alloy for an improved ductility. In most cases, a pure Al or Ni interlayer, ~50 μm thick, is incorporated between the bearing alloy and steel backing to prevent deleterious intermetallic phase formation at the interface during heat treatment. A variety of intermediate heat treatments is also used to stress relieve the composite structure, to modify the morphology of the second phases (typically, a reticular network of Sn islands, 10 to 20 m in size, interconnected along the trigonal grain boundaries), or an age-hardening procedure (Ref 2).

In the quest for overlays with improved combinations of properties, high-velocity oxyfuel (HVOF) thermal spraying has been demonstrated in previous studies to be an attractive alternative route for manufacturing Al-Sn-based bearing layers (Ref 4). This rapid solidification process allows low-porosity Al-Sn-based layers to be deposited directly onto a steel strip for potential use in journal bearings. For the case of alloys having a limited solubility, rapid solidification processing is expected to affect the mechanical properties through microstructural refinement, the extension of solid solubility, or the formation of non-equilibrium phases. This, in turn may improve the alloy strength, and enhance both fatigue and wear resistance (Ref 5). The

This article was originally published in *Building on 100 Years of Success, Proceedings of the 2006 International Thermal Spray Conference* (Seattle, WA), May 15-18, 2006, B.R. Marple, M.M. Hyland, Y.-Ch. Lau, R.S. Lima, and J. Voyer, Ed., ASM International, Materials Park, OH, 2006.

T. Marrocco, L.C. Driver, S.J. Harris, and **D.G. McCartney,** University of Nottingham, Nottingham, UK. Contact e-mail: emxtm@nottingham.ac.uk.

HVOF thermal spray process is characterized by a rapid cooling rate of splats, which is typically 10^6 K/s (Ref 6), and in AlSn-based alloys the as-sprayed microstructure was found to comprise a supersaturated Al matrix and a nanoscale Sn particle dispersion (Ref 7).

To further improve the bearing performance of these thermally sprayed alloys, consideration needs to be given to other possible alloy additions. The current study extends previous work on ternary Al-Sn-Cu alloys to quaternary systems, with specific additions of a fourth element for enhancement of the properties of the deposit. Two alloys were studied in detail: Al-20wt.%Sn-1wt.%Cu-2wt.%Ni (Al20Sn1Cu2Ni); and Al-20wt.%Sn-1wt.%Cu-7wt.%Si (Al20Sn1Cu7Si). The aims of this work were to elucidate the microstructures of the deposits produced by HVOF spraying and to determine the effect of a short annealing heat treatment on microstructural development, microhardness, and wear properties. Wear behavior was characterized using the automotive industry standard Viper test (Ref 8), which employs hot engine oil as a lubricant.

2. Experimental Methods

2.1 Materials

The powders used for spraying, Al20Sn1Cu2Ni and Al20Sn1Cu7Si, were produced by inert gas atomization (N_2) in a nominal size range of −45 to +25 μm and were supplied by PSI Ltd. (Sussex, UK). Actual particle size distributions were obtained by using laser diffractometry (Mastersizer S; Malvern Instruments, Malvern, UK). The mass mean particle size, determined by laser diffractometry, was 36 μm for both powders. The substrate material was mild steel (BS080A15) in the form of rectangular coupons (58 × 25 × 2 mm), which were grit blasted with alumina grit prior to deposition.

2.2 High-Velocity Oxyfuel Thermal Spraying

Thermal spraying was undertaken using a Metallisation (Dudley, West Midlands, UK) Met Jet II HVOF system using liquid fuel (kerosene). This HVOF system has been described in detail elsewhere (Ref 9).

Briefly, the fuel used is liquid kerosene, which is combusted with pure oxygen at a pressure of around 8 bar in the combustion chamber of the gun. The combustion products flow through a converging-diverging nozzle, and the powder is injected into the hot, high-speed gas just downstream of the throat through two radial ports. The powder is thus accelerated and heated by the gas stream as it flows along a parallel-sided barrel before exiting the gun. In the present work, the substrates to be coated were mounted onto a rotating carousel, and the rotation speed was chosen so that the substrates traversed the spray path at a horizontal speed of ~1 m/s. The gun was traversed vertically at a speed of 5 mm/s in a series of 40 passes to achieve deposits that were typically 200 to 300 μm thick. During deposition, the average substrate temperature was maintained below 190 °C using compressed air jets. Table 1 summarizes the parameters used in this study, which were optimized to minimize deposit porosity and to achieve a suitable deposit microhardness.

2.3 Deposit Heat Treatment

Following spray deposition, the samples (i.e., coating plus substrate) were heat treated at 300 °C (i.e., above the melting point of pure Sn to allow for controlled Sn coarsening (Ref 10) and precipitation of Sn within the Al matrix) for various times (i.e., 1–5 h) and then were air cooled to room temperature. Heat treatments were conducted in a fan oven, the internal temperature of which was monitored by a thermocouple.

2.4 Wear Test Method

The wear testing of the heat-treated deposits was carried out at Dana Glacier Vandervell (Rugby, UK), where the industry standard Viper test rig (Ref 8), shown schematically in Fig. 1, was used. The shaft rotation speed was 1000 rpm, and a load of 2.2 kg was applied. It was possible to test three samples at a time along the length of the shaft. The test duration was 30 min. To prepare the samples for wear testing, they were wet cut into square pieces 15 × 15 mm in size from the sprayed and heat-treated coupons using a diamond saw. The specimens were dry ground using 1200-grade SiC paper to remove the as-sprayed surface roughness and to provide a consistent surface finish for the wear testing.

2.5 Microstructural Characterization of Powders and Coatings

A Jeol 6400 (Jeol Ltd., Tokyo, Japan) scanning electron microscope (SEM) operated in high-vacuum mode was used to examine the microstructures of the powders, as-sprayed and heat-treated deposits, using the backscattered electron (BSE) signal to form images. Qualitative energy dispersive x-ray analysis was also used to aid phase identification. For the purpose of cross-sectional microstructural investigation, coated samples were mounted in conducting resin, and were sequentially ground and polished to a 1 μm surface finish. To examine powder cross sections, a small number of particles were also mounted in a con-

Table 1 Spray conditions for the Al20Sn1Cu2Ni and Al20Sn1Cu7Si powders using the Met Jet II gun

Parameter	Value
Kerosene flow rate, L/min	0.25
Oxygen flow rate, L/min	755
Carrier gas flow rate, L/min	5.5
Powder feed rate, g/min	10.5
Substrate velocity (horizontal plane), m/s	1
Barrel length, mm	100

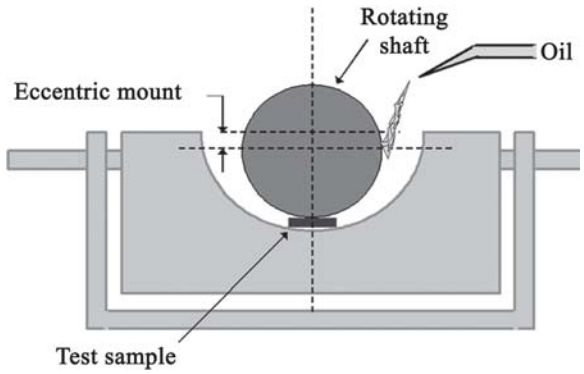

Fig. 1 Schematic illustration of the Viper test rig

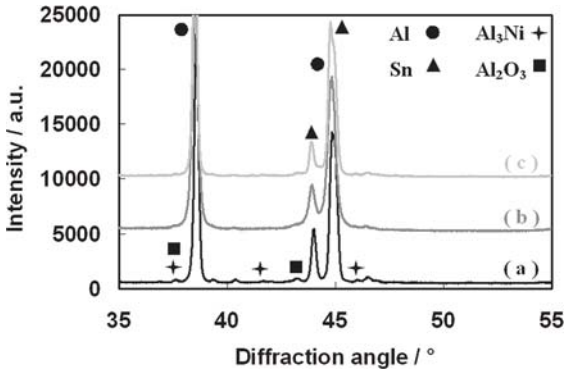

Fig. 2 (a) XRD spectra of the 2 wt.% Ni-containing powder, (b) the as-sprayed coating, and (c) the heat-treated coating

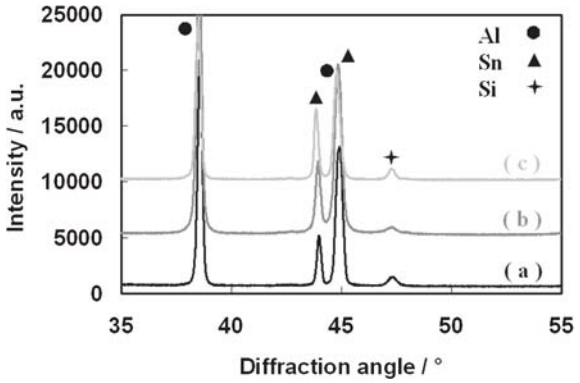

Fig. 3 (a) XRD spectra of the 7 wt.% Si-containing powder, (b) the as-sprayed coating, and (c) the heat-treated coating

ductive resin. Specimens were ground on wet 1200-grade SiC grit without exercising too much pressure, and were polished with 6 and 1 μm diamond paste for a few seconds using paraffin as lubricating medium. Polished samples were stored in a dessicator prior to examination to prevent surface degradation in the atmosphere. The microstructure of the worn samples was also studied by examining their top surface using the SEM in both the secondary electron (SE) and BSE modes.

X-ray diffraction (XRD) analysis with monochromatic Cu-Kα radiation (λ = 0.15406 nm) was used for phase identification in starting powders, as-sprayed and heat-treated deposits. The diffractometer was operated at 40 kV and 20 mA with diffraction angles (2θ) ranging from 20 to 140°. A 0.05° step size and a 2 s counting time at each step were used. A limited number of samples were examined in more detail using a 0.01° step size, an 8 s counting time in the range of 35 to 55°. Phases present in the spectra were identified with the aid of Joint Committee on Powder Diffraction Standards diffraction files.

Microhardness tests were also performed on polished cross sections of the coatings, in the as-sprayed condition and after heat treatment, using a Leco M-400 instrument (Saint Joseph, MI) with a 200 gf load and 15 s loading time. This produced an indentation size, point to point, of ~25 to 50% of the coating thickness, depending on the heat-treated condition of the coating. The mean microhardness values were obtained from a series of 10 indentations taken along the midplane of the coating transverse section on each specimen.

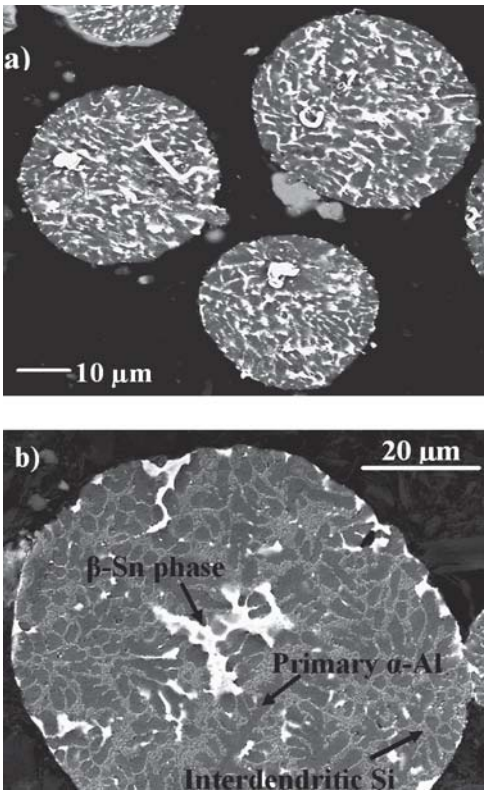

Fig. 4 BSE images showing the microstructure of (a) the Ni-containing powder and (b) the Si-containing powder, etched using a 0.5% HF solution

3. Results

Figures 2 and 3 show the XRD spectra of Ni- and Si-containing powders, as-sprayed and annealed coatings, respectively. The main peaks identified in the XRD patterns of both powders are attributed to Al and Sn. The Ni-containing powder (Fig. 2) exhibited several peaks from minor phases, in addition to the main phases Al and body-centered tetragonal Sn, which were identified as Al_3Ni and Al_2O_3. The additional peaks present in the Si-containing powder (Fig. 3) were attributed to Si.

Following deposition of the coatings, the main Al and Sn peaks remained in similar proportions in both cases. The as-sprayed Ni-containing coating (Fig. 2) showed a decrease in the quantity of secondary phases present. In the as-sprayed Si-containing coating (Fig. 3), Al, Sn, and Si were all detected, but the quantity of Si was reduced compared with that in the original powder. After the heat treatment at 300 °C for 1 h, all of the coatings exhibited a small increase in the amount of secondary phases present.

Figure 4 shows the cross sections of the powders, which are seen to be circular, consistent with a near-spherical morphology expected from a gas-atomized powder. The image of the Ni-containing powder (Fig. 4a) reveals a characteristic structure of Al-rich dendrites (dark) surrounded by an Sn-rich interdendritic

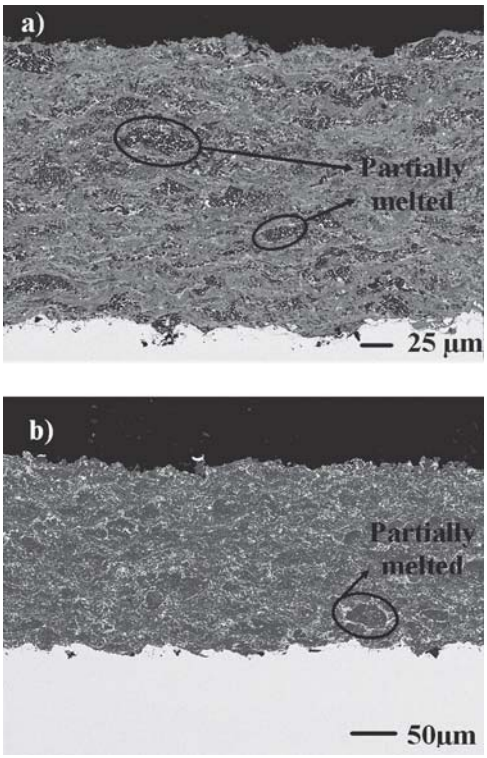

Fig. 5 BSE images of the cross section of the as-sprayed (a) Ni-containing coating and (b) Si-containing coating

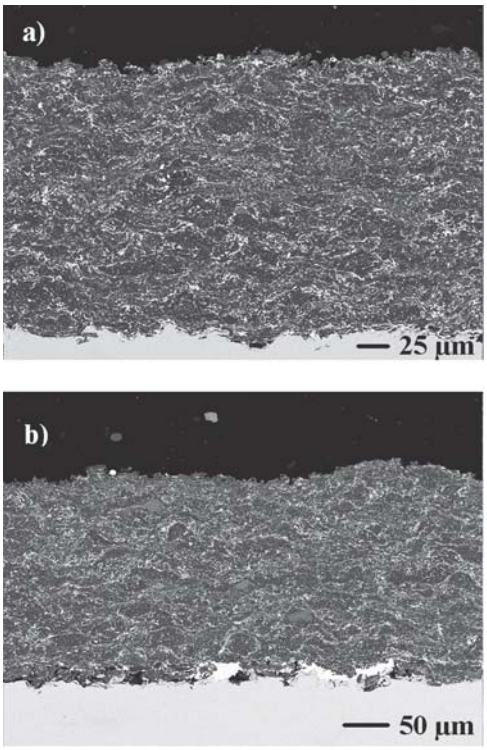

Fig. 6 BSE images of the cross section of the heat-treated (at 300 °C for 1 h) (a) Ni-containing coating and (b) Si-containing coating

phase (light), with the Sn phase randomly distributed throughout the particle. The phase $NiAl_3$ identified by XRD could not be detected using SEM. In the case of the Si-containing powder (Fig. 4b), Sn is not homogeneously distributed; instead, there are only a small number of coarse areas of Sn. Etching has revealed the dendritic structure of the αAl phase, and Si is seen to be present with a fine-scale eutectic-like morphology between the Al dendrites.

Figure 5(a) and (b) show BSE images of typical cross sections of the as-sprayed Ni- and Si-containing coatings, respectively. Generally, a relatively featureless microstructure is observed in the SEM images with only small amounts of Sn-rich phase (white) distributed throughout the coating. The Sn-rich phase is present both within the splats themselves, where it appears to be submicron in size, and also along the intersplat boundaries in elongated forms of ~1 µm thickness. It is evident that powder particles that were not fully melted were incorporated into the coating. Differences between the two types of coatings are evident in terms of these partially melted particles.

The cross sections of the heat-treated Ni- and Si-containing coatings, as seen in Fig. 6(a) and (b), respectively, show how the Sn within the deposit agglomerates and coarsens. This is particularly evident in the AlSnCuNi coating. The Sn-rich phase coarsens within all regions of the coating following heat treatment, which makes the structures of the partially melted powder particles less evident in both types of coatings.

Figure 7 shows the effect of the heat treatment on the microhardness of the coatings as a function of the annealing time. Initially, the Si-containing coating is slightly harder than the one containing Ni. Both coatings show a significant decrease in microhardness within the first 30 min of heat treatment, after which time the Ni-containing coating maintains higher values of hardness.

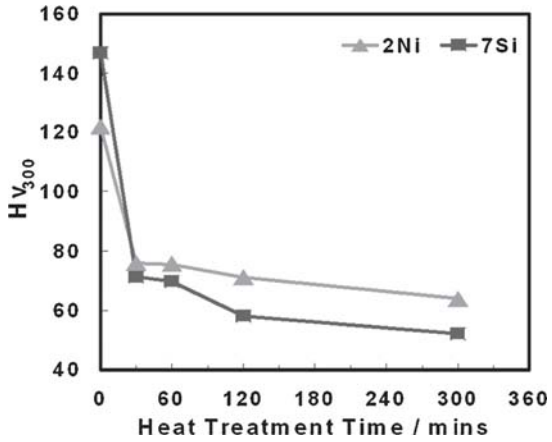

Fig. 7 Variation of the microhardness with heat treatment time following annealing at 300 °C

Figure 8 is a scatterplot showing the specific weight loss (in micrograms per meter) of the Al20Sn1Cu2Ni and Al20Sn1Cu7Si obtained from the present work along with data from a previous study on the HVOF-sprayed ternary alloy Al20Sn1Cu. It is clear that the coatings sprayed using Ni-containing powder produced an average loss of ~6 to 9 µg/m, whereas the Si-containing coating performed significantly better, showing lower weight loss of ~4 µg/m. For the ternary alloy,

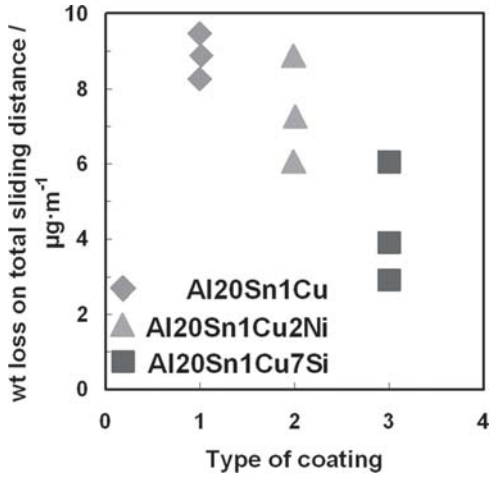

Fig. 8 Weight loss data from the Viper test after 30 min, showing a comparison between the original ternary Al20Sn1Cu alloy and the quaternary alloys of the present work

the weight loss was higher compared with both quaternary alloys (>9 µg/m).

Plan view images of the wear scar from the Al20Sn1Cu2Ni alloy are shown in Fig. 9. The SE image of Fig. 9(a) shows a sharp interface between worn and unworn regions, where the scratches, arising from the previous grinding and polishing used to prepare the surface prior to the wear testing, have disappeared in the worn area. The directional nature of the test due to the rotating shaft is also evident, leaving clear left-to-right markings. The BSE image of the interface (Fig. 9b) shows the Sn (white) smeared in the same direction as the shaft rotation.

4. Discussion

In the rapidly solidified, gas-atomized powder, the quantity of the intermetallic compound (Al_3Ni) was just sufficient to be detected by XRD analysis, whereas this was not the case for the as-sprayed deposit, as evidenced in Fig. 2. However, following heat treatment at 300 °C, an increase in the volume fraction of such a precipitate occurred, as the increased intensity of the Al_3Ni peaks in the XRD pattern of the heat-treated deposit confirm. The XRD patterns in Fig. 3 show that, in the Si-containing powder, the Si peaks were of low intensity and rather broad, indicating a small volume fraction of this phase with a fine grain size and/or significant microstrain (Ref 11). The as-sprayed deposit gave an XRD pattern with well-defined peaks from Al and Sn, but in this case the Si peaks were evident only during the slow scan from 35 to 55°. Following annealing, the deposit gave an XRD pattern that was similar to that of the powder, but the Si peaks were of marginally greater intensity and somewhat narrower in width. These differences indicate that, in the as-sprayed condition, more of the Si was retained in solid solution in the αAl matrix than was the case with the powder. Furthermore, the precipitation of Si from this supersaturated αAl would seem to have occurred during annealing.

It is evident that the powders have a microstructure that is very different from the as-sprayed coating. This is attributed to

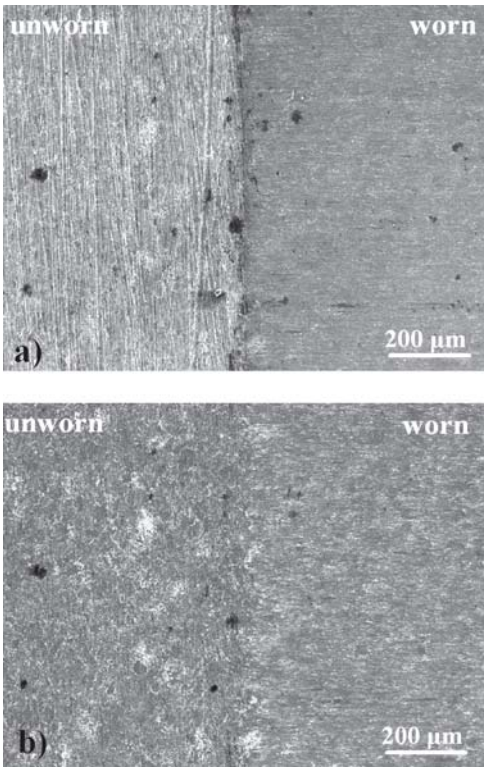

Fig. 9 SEM images of the worn Ni sample (plan view of the wear scar): (a) SE image; and (b) BSE image

the different cooling rates experienced and to the nature of the Al-Sn phase diagram. Depending on the particle diameter, powders cool at ~10^3 to 10^5 K/s when gas atomized, whereas the cooling rate of splats is ~10^6 to 10^7 K/s during thermal spraying. It is reasonable to base an explanation of solidification behavior on the Al-Sn phase diagram (Ref 12, 13), which exhibits a metastable liquid-phase miscibility gap. At the lower cooling rates of gas atomization, the formation of primary solid αAl occurs as predicted by the equilibrium phase diagram, whereas at the higher cooling rates of splats a phase separation of dispersed liquid Sn droplets in molten Al occurs initially as indicated by the metastable diagram. Therefore, gas-atomized AlCuSnNi powders solidify with primary αAl dendrites and interdendritic Sn; small amounts of $NiAl_3$ may form during the latter stages of freezing. The 7 wt.% Si in the AlSnCuSi alloy powder (eutectic composition ~12 wt.% in the Al-Si system) gives rise to the growth of Al-Si eutectic cells between primary αAl dendrites with the rejection of Sn into the residual liquid. This segregated Sn-rich liquid freezes as isolated pools of Sn (Fig. 4b). In as-sprayed deposits of both alloys, the initial nanoscale Sn-droplet dispersion is retained to room temperature by rapid growth of the αAl phase during splat cooling, which traps the Sn-rich droplets. The latter then solidify to an Sn-rich phase at a temperature below 232 °C. The secondary phase, that is Si or $NiAl_3$, could form either from the melt or by solid-state precipitation.

The microhardness of the as-sprayed coatings has been found to be higher (>100 kgf/mm^2) compared with the microhardness of the powder (65 kgf/mm^2). One reason for this change is the presence of phases distributed on a submicron and nanoscale

level within the solidified Al grains. Another reason is the existence of dislocation tangles introduced either by the rapid cooling rate or as a result of the deformation produced by the high-velocity impact of the powder particles on the substrate during HVOF spraying (Ref 10). The same coatings were then heat treated at 300 °C for different times. Heat treatment lowers the microhardness, coarsening the Sn particles. This significant decrease in hardness following short annealing times can be attributed to the rapid coarsening of the submicron precipitates in the as-sprayed coating. In practice, for bearing materials, a hardness of 60 to 65 kgf/mm^2 is required, to allow both proper forming of the bearing and also to give desired in-service performance.

In terms of wear test results (Fig. 8), an important point to note is that Si improves wear resistance more than Ni, when compared with the Al20Sn1Cu coating. This is probably due to the presence of hard Si particles within the structure, which are present in a higher volume percent than those of the $NiAl_3$ phase, which is also of lower hardness. The BSE image of the interface between worn and unworn regions (Fig. 9b) shows the Sn (bright) smeared in the same direction as the shaft rotation, showing a marked orientation effect and demonstrating the antiseizure properties of the soft Sn. The presence of low levels of porosity, resulting from spraying, is also evident. However, the surface appears to wear uniformly with no evidence of splat decohesion and removal.

5. Conclusions

Deposits formed by HVOF spraying of quaternary Al-Sn-based alloys have microstructures that differ significantly from those of the gas-atomized feedstock powders. The powder microstructures contain Al-rich dendrites and micron-sized regions of Sn, whereas the deposits exhibit a fine-scale, submicron dispersion of Sn particles within an αAl matrix.

The difference in solidification morphology is attributed to the higher cooling rate of HVOF splats compared with the gas-atomized powder combined with the presence of a metastable liquid-phase miscibility gap in the Al-Sn phase diagram, which is reached only at sufficiently high cooling rates.

Annealing at 300 °C causes the dispersed Sn phase to coarsen in both types of alloys. It also increases the fraction of $NiAl_3$ and Si precipitates in the Ni- and Si-containing coatings, respectively, compared with the as-deposited alloy.

In the as-sprayed condition, coating microhardnesses of 120 and 150 kgf/mm^2 are attained for the Ni- and Si-containing alloys, respectively. In both materials, the hardness decreases with an increase in the annealing time, and this is attributed to a number of factors including dispersed Sn-phase coarsening, coarsening of Si or $NiAl_3$ precipitates, and loss of solid solution-strengthening effects.

The wear resistance of the AlSnCuSi alloy is significantly higher than either an AlSnCu or an AlSnCuNi alloy. This is possibly due to the presence of submicron, hard Si-phase particles in the AlSnCuSi alloy.

Acknowledgments

The authors acknowledge support from Engineering and Physical Sciences Research Council (EPSRC) and Dana Glacier, and thank Andrew Horlock for spraying and Carl Perrin for help with the Viper testing.

References

1. Materials for Sliding Bearings, Vol. 3, *ASM Handbook* (formerly *Metals Handbook,* 9th ed.), ASM International, 1980, p 802-822
2. S. Abis, G. Onofrio, and E. Signorelli, *New Bearing Al-Based Alloys: Evolution of Advanced Materials,* Associazione Italiana Di Metallurgia, Federal Mogul, Italy, 1989, p 511-516
3. A.H. Sully, H.K. Hard and T.J. Heal, *J. Inst. Met.,* 1949/1950, **LXXVI,** p 269-294
4. C. Perrrin, D.G. McCartney, S.J. Harris, and A.J. Sturgeon, Forming a Plain Bearing Lining, U.S. Patent 6,416,877, July 9, 2002
5. H. Jones, *Rapid Solidification of Metals and Alloys,* Institution of Metallurgists, London, 1982
6. R.P. Krepski, *Thermal Spray Coating Applications in the Chemical Process Industries,* NACE International, 1993
7. C. Perrrin, S.J. Harris, D.G. McCartney, S. Syngellakis, and P.A.S. Reed, The Potential of New Processing Routes in Al-based Plain Journal Bearings, *Aluminium Alloys: Their Physical and Mechanical Properties*, *Proceedings of the 9th International Conference of Aluminium Alloys,* J.F. Nie, A.J. Morton, and B.C. Muddle, Ed., 2004, (Melbourne, Australia), Institute of Material Engineering, Australasia LDT, 2004, p 1371-1376
8. T. Marrocco, "Wear of Thermally Sprayed Al-Sn Based Alloys," Master's Thesis, Politecnico di Torino, 2003
9. D. Zhang, D.G. McCartney, and S.J. Harris, Microstructure Formation and Corrosion behaviour in HVOF-sprayed Inconel 625 Coatings, *Mater. Sci. Eng., A,* 2003, **344,** p 45-56
10. C.J. Kong, P.D. Brown, A.J. Horlock, S.J. Harris, and D.G. McCartney, Microstructural Characteristics of High Velocity Oxy-Fuel Thermally Sprayed Al-12wt.%Sn-1wt.%Cu Alloys, *Inst. Phys. Conf. Ser. No.* 168, M. Aindow and C.J. Kiely, Ed., Electron Microscopy and Analysis 2001, Institute of Physics, London, UK, 2001, p 227-230
11. B.D. Cullity, *Elements of X-Ray Diffraction,* Addison-Wesley, Reading, MA, 1978
12. B. Predel, *Landolt-Börnstein-Group IV Physical Chemistry*, Vol 5, *A, Al-Sn*, Springer-Verlag, Heidelberg, 1991
13. C.J. Kong, P.D. Brown, S.J. Harris, and D.G. McCartney, The Microstructures of a Thermally Sprayed and Heat-Treated Al-20wt%Sn-3wt%Si Alloy, *Mater. Sci. Eng., A*, 2005, **403,** p 205-214